

# Ambipolar Drift Heating in Turbulent Molecular Clouds

Paolo Padoan

Harvard University Department of Astronomy, Cambridge, MA 02138,  
padoan@cfa.harvard.edu

Ellen Zweibel

JILA, University of Colorado at Boulder, Boulder CO 80309-440,  
zweibel@solarz.colorado.edu

Åke Nordlund

Astronomical Observatory and Theoretical Astrophysics Center, Juliane Maries Vej 30,  
DK-2100 Copenhagen, Denmark, aake@astro.ku.dk

Received \_\_\_\_\_; accepted \_\_\_\_\_

## ABSTRACT

Although thermal pressure is unimportant dynamically in most molecular gas, the temperature is an important diagnostic of dynamical processes and physical conditions. This is the first of two papers on thermal equilibrium in molecular clouds. We present calculations of frictional heating by ion-neutral (or ambipolar) drift in three-dimensional simulations of turbulent, magnetized molecular clouds.

We show that ambipolar drift heating is a strong function of position in a turbulent cloud, and its average value can be significantly larger than the average cosmic ray heating rate. The volume averaged heating rate per unit volume due to ambipolar drift,  $H_{AD} = |\mathbf{J} \times \mathbf{B}|^2 / \rho_i \nu_{in} \sim B^4 / (16\pi^2 L_B^2 \rho_i \nu_{in})$ , is found to depend on the rms Alfvénic Mach number,  $\mathcal{M}_A$ , and on the average field strength, as  $H_{AD} \propto \mathcal{M}_A^2 \langle |B| \rangle^4$ . This implies that the typical scale of variation of the magnetic field,  $L_B$ , is inversely proportional to  $\mathcal{M}_A$ , which we also demonstrate.

## 1. Introduction

Observations reveal that roughly 20% - 40% of the interstellar gas in the Galactic disk is organized into Giant Molecular Clouds (GMCs). These clouds appear to be self gravitating and roughly in virial equilibrium. The density distribution in the clouds is highly inhomogeneous, and the velocity field is turbulent and highly supersonic. It is thought that both magnetic and turbulent kinetic pressure contribute to cloud support, but the relative degree of magnetic support is uncertain because of the observational difficulty of measuring the magnetic field strength and topology.

Several lines of evidence suggest that GMCs survive for a few tens of millions of years, but both analytical estimates, some dating back more than two decades (Goldreich & Kwan 1974, Field 1978, Zweibel & Josafatsson 1983, Elmegreen 1985), and numerical simulations (Scalo & Pumphrey 1982, Stone, Ostriker, & Gammie 1998, MacLow 1999, Padoan & Nordlund 1999) suggest that molecular cloud turbulence dissipates in much less than the cloud lifetime. Star formation is observed to take place in nearly all GMCs, and it appears that the lifetimes of GMCs are determined by the rate at which they are destroyed by energy and momentum input from the massive stars which form within them. It also appears likely that energy input from stars, and possibly from other sources, drives turbulence in GMCs as well.

Ambipolar drift, or ion-neutral friction, has long been thought to be an important energy dissipation mechanism in molecular clouds, and therefore a significant heating mechanism for molecular cloud gas (Scalo 1977, Goldsmith & Langer 1978, Zweibel & Josafatsson 1983, Elmegreen 1985). In fact, as first suggested by Scalo (1977), the observed low temperatures of molecular clouds places upper limits on the rate of energy dissipation by ambipolar drift, and thus, with some additional assumptions, on the magnetic field strength.

Nevertheless, it has been difficult to assess the rate of energy dissipation by ambipolar drift. The frictional heating rate  $H_{AD}$  depends on the local Lorentz force in the medium, which is almost impossible to measure. Simple scaling arguments show that  $H_{AD}$  is proportional to  $B^4 n^{-1} n_i^{-1} L_B^{-2}$ , where  $B$ ,  $n$ ,  $n_i$ , and  $L_B$  are the magnetic field strength, neutral density, ion density, and magnetic length scale, respectively. The extreme sensitivity of this formula to magnetic field strength, only the line of sight average value of which can be directly measured, and to the essentially unobservable  $L_B$ , has made it difficult to estimate  $H_{AD}$  with confidence even to order of magnitude.

In this paper, we use numerical simulations of magnetized turbulence to study heating by ambipolar drift in molecular clouds. We show that the ambipolar heating rate per unit volume,  $H_{AD}$ , depends on field strength as  $B^4$ , for constant rms Mach number of the flow, and on the Alfvénic Mach number as  $\mathcal{M}_A^2$ . This implies that the magnetic length scale,  $L_B$ , depends on the Alfvénic Mach number as  $\mathcal{M}_A^{-1}$ , which we demonstrate. We show that the numerical value of the heating rate, computed by solving the three-dimensional compressible magneto-hydrodynamic (MHD) equations, tends to converge with increasing numerical resolution, and therefore we can fully quantify the value of  $H_{AD}$ , to within an uncertainty of less than a factor of two, in the numerical models.

These empirical formulae make it much easier to estimate ambipolar drift heating in terms of observable properties of clouds. The average heating rate depends on  $B^2$ , rather than  $B^4$  as in the traditional expression, on the line width or rms velocity, and on the neutral and ion densities. The magnetic length scale is eliminated through its dependence on  $\mathcal{M}_A$ .

We find that ambipolar drift is probably a stronger heating mechanism than cosmic ray heating, and that it is a strong damping mechanism for molecular cloud turbulence, leading to significant decay within one dynamical crossing time.

In §2 of the paper we briefly summarize the physics of ambipolar drift heating, and in §3 we describe the simulations. In §4 we present results of the computation of ambipolar drift heating rate, and in §5 we discuss some implications of the results and summarize the conclusions of this work.

## 2. Dynamics and Dissipation of Weakly Ionized Gas

Molecular cloud gas includes neutral atoms and molecules, atomic and molecular ions, electrons, and dust grains, which may also be electrically charged. At the gas densities considered in this paper ( $0.1 \text{ cm}^{-3} < n < 10^5 \text{ cm}^{-3}$ , and  $\langle n \rangle = 320 \text{ cm}^{-3}$ ), electrons are the primary current carriers, the number density of ions much exceeds the number density of grains, and Ohmic dissipation is negligible (Nakano & Umebayashi 1986). Moreover, significant charge separation cannot be sustained on the time scales and length scales of interest, so the electrons and ions move together. The electric field is then given by

$$\mathbf{E} = -\frac{\mathbf{v}_i}{c} \times \mathbf{B}, \quad (1)$$

where  $\mathbf{v}_i$  is the velocity of the ion, or plasma component.

In principle,  $\mathbf{v}_i$  and the neutral velocity  $\mathbf{v}_n$  should be determined by solving separate fluid equations for these species (Draine 1986), including their coupling by collisional processes. In typical molecular cloud environments this leads to a great disparity of length scales and time scales, because ions collide with neutrals at a very high frequency compared to other rates in the problem. Past computations of two fluid systems (Toth 1994, Brandenburg & Zweibel 1995, Hawley & Stone 1998) have avoided this problem by assuming ion to neutral density ratios that are far higher than the values found in typical

molecular clouds. An alternative, which we pursue here, is to consider only the length scales and time scales over which the ions and neutrals are well coupled (Shu 1983).

We introduce the drift velocity  $\mathbf{v}_D$

$$\mathbf{v}_D \equiv \mathbf{v}_i - \mathbf{v}_n \quad (2)$$

and evaluate  $\mathbf{v}_D$  by assuming that the dominant forces on the charged component are the Lorentz force and the frictional force arising from collisions with neutrals. We model the latter in the standard way as

$$F_{in} = -\rho_i \nu_{in} \mathbf{v}_D, \quad (3)$$

where  $\rho_i \nu_{in} = \rho_n \nu_{ni} = \rho_i \rho_n \langle \sigma v \rangle / (m_i + m_n)$ . In numerical work, we will take the collision rate coefficient  $\langle \sigma v \rangle = 2 \times 10^{-9} \text{ cm}^3/\text{s}$  (Draine, Roberge, & Dalgarno 1983) and assume the ions are  $\text{HCO}^+$  (cf. de Jong, Dalgarno, & Boland 1980) and the neutrals are  $\text{H}_2$  and  $\text{He}$ , with  $n(\text{He})/n(\text{H}_2) = 2/9$ . On time scales longer than the neutral-ion collision time  $1/\nu_{ni}$ , the Lorentz and drag forces must balance. This leads to an expression for the drift velocity

$$\mathbf{v}_D = \frac{\mathbf{J} \times \mathbf{B}}{c\rho_i \nu_{in}}. \quad (4)$$

Making the further assumption  $\rho_i/\rho \ll 1$ , so that  $\mathbf{v}_n$  is the same as the center of mass velocity  $\mathbf{v}$ , the magnetic induction equation is

$$\frac{\partial \mathbf{B}}{\partial t} = \nabla \times (\mathbf{v}_i \times \mathbf{B}) = \nabla \times (\mathbf{v} \times \mathbf{B}) + \nabla \times \frac{(\mathbf{J} \times \mathbf{B}) \times \mathbf{B}}{c\rho_i \nu_{in}}. \quad (5)$$

The frictional heating rate  $H_{AD}$  is

$$H_{AD} = \rho_i \nu_{in} | \mathbf{v}_D |^2 . \quad (6)$$

Equations (4), (5), and (6) constitute the strong coupling approximation to ambipolar drift. They are much easier to solve, and at less computational expense, than the full two fluid equations that hold for even a single neutral species and a single charged fluid. Nevertheless, we must consider where these equations break down. The validity of the strong coupling approximation, even at low drift velocities, can be assessed by evaluating the ambipolar Reynolds number  $R_{AD}$  (Zweibel & Brandenburg 1997)

$$R_{AD} \equiv \frac{L_B v \nu_{ni}}{v_A^2} \sim \frac{v}{v_D}, \quad (7)$$

where  $L_B$  is the length scale on which the magnetic field varies, and in the second relation we have used eqn. (4). The strong coupling approximation should be valid for  $R_{AD} \gtrsim 1$ . As examples, this criterion gives the wavenumber for critical damping of small amplitude MHD waves of wavelength  $\lambda$  if we replace  $v$  by  $v_A$  and  $L_B$  by  $\lambda/\pi$  in eqn. (7) (McKee et al. 1993). And, the criterion for significant ion-neutral separation in shocks (Mullan 1971, Draine 1980) is equivalent to the condition  $R_{AD} < 1$  evaluated upstream.

We show in §4 that  $L_B \propto \mathcal{M}_A^{-1}$ , where  $\mathcal{M}_A$  is an appropriately averaged Alfvén Mach number defined in eqn. (24). Therefore,  $R_{AD} \propto \mathcal{M}_A$ : we expect that, on average, the strong coupling approximation is increasingly good as  $\mathcal{M}_A$  increases. For example, in our  $N = 128^3$  simulations, the value of  $R_{AD}$  spans a range from about 5 to about 300, for  $0.5 \leq \mathcal{M}_A \leq 30$ . In practice, however,  $L_B$  is bounded below by the resolution of the grid, leading to a flattening of the  $L_B$  vs  $\mathcal{M}_A$  relation as  $\mathcal{M}_A$  increases. This can be seen in

Figure 3 for  $\mathcal{M}_A \gtrsim 10$ . Thus, although we do not accurately model MHD shocks in which two fluid effects are significant (see Draine & McKee 1993), we do resolve much of the magnetic field structures outside of shocks, at least in simulations with  $\mathcal{M}_A < 10$ .

### 3. The Simulations

The code and basic equations it solves have been previously described in Nordlund, Stein & Galsgaard (1996), Nordlund & Galsgaard (1997), Padoan et al. (1998), and Padoan & Nordlund (1999). Here, we include ambipolar drift, in the strong coupling approximation described in §2, for the first time, but this has not required changes in the numerical method.

The code solves the compressible MHD equations on a 3-dimensional staggered mesh, with volume centered mass density and thermal energy, face centered velocity and magnetic field components, and edge centered electric currents and electric fields (Nordlund, Stein & Galsgaard 1996):

$$\frac{\partial \ln \rho}{\partial t} + \mathbf{v} \cdot \nabla \ln \rho = -\nabla \cdot \mathbf{v}, \quad (8)$$

$$\frac{\partial \mathbf{v}}{\partial t} + \mathbf{v} \cdot \nabla \mathbf{v} = -\frac{P}{\rho} \nabla \ln P + \frac{1}{c\rho} \mathbf{J} \times \mathbf{B} + \mathbf{f}, \quad (9)$$

$$P = \rho T, \quad (10)$$

$$\frac{\partial \mathbf{B}}{\partial t} = \nabla \times (\mathbf{v} \times \mathbf{B}) + \nabla \times \frac{(\mathbf{J} \times \mathbf{B}) \times \mathbf{B}}{c\rho_i \nu_{in}}. \quad (11)$$



$$\frac{4\pi}{c}\mathbf{J} = \nabla \times \mathbf{B}, \quad (12)$$

plus numerical diffusion terms, and with periodic boundary conditions. The system is forced by  $\mathbf{f}$ , an external random driver, and all the other symbols have their usual meanings.

In calculating the dynamics we use an isothermal equation of state, as in our previous work, even though in this paper and the next we are concerned with the thermal equilibrium of the gas, and preliminary results suggest a significant spread of temperatures. As long as the motions remain highly supersonic, the dynamics should be almost insensitive to the thermal pressure, although the equation of state certainly affects the density contrast produced in shocks.

We use spatial derivatives accurate to 6th order, interpolation accurate to 5th order, and Hyman’s 3rd order time stepping method (Hyman 1979). The code uses shock and current sheet capturing techniques to ensure that magnetic and viscous dissipation at the smallest resolved scales provide the necessary dissipation paths for magnetic and kinetic energy. As shown by Galsgaard & Nordlund (1996, 1997), dissipation of magnetic energy in highly turbulent, compressible MHD plasmas occurs at a rate that is independent of the details of the small scale dissipation. In ordinary hydrodynamic turbulence the corresponding property is one of the cornerstones of Kolmogorov (1941) scaling.

The initial random velocity field is generated in Fourier space, with a normal distribution of amplitudes and random phases, and with power only in the Fourier components in the shell of wave-number  $1 \leq kL/2\pi \leq 2$ . In all but one of the experiments the flow is driven by an external random force ( $\mathbf{f}$  in the momentum equation (9)). The random force is also generated in Fourier space with a normal distribution, with power only in the range of wave-number  $1 \leq kL/2\pi \leq 2$ . A Helmholtz decomposition is performed on both the initial velocity and the random force, and only the solenoidal component is used.

In order to produce a force that varies continuously in time, we actually specify randomly distributed Fourier components of the time derivative of the acceleration, and compute the acceleration as a time integral. The time derivative of the Fourier components of the acceleration are regenerated at time intervals of about one dynamical time.

All our models have periodic boundary conditions. This is an efficient way to study the evolution of MHD turbulence under internal forces, but it precludes study of the coupling between molecular clouds and the surrounding diffuse medium, such as, for example, outward radiation of cloud energy in the form of MHD disturbances (Elmegreen 1985). Since we do not have a physically motivated model for the initial conditions, we allow the models to relax before studying their statistical properties, and report only results for the steady state.

For the purpose of computing the ambipolar drift heating rate, we have run several experiments with external random driving, at an approximately constant sonic rms Mach number,  $\mathcal{M} \approx 10$ , with different values of the magnetic field strength, in a  $128^3$  numerical grid (named A1 to A7 in Table 1), and a decaying experiment (no external driving), with approximately constant value of the rms Alfvénic Mach number,  $\mathcal{M}_A \approx 1$ , and magnetic field strength that decreases with time (named B1 in Table 1). In order to perform a convergence study, we have repeated a  $128^3$  experiment at lower resolutions:  $64^3$ ,  $32^3$ , and  $16^3$  (experiments A4 in Table 1). Finally, we have repeated a  $128^3$  experiment with different values of the ambipolar drift parameter  $a$ , introduced below (experiments A3 in Table 1). The results of these experiments are presented in the next section, and some of their parameters are listed in Table 1. When we rescale the experiments to physical units (see below) we use an average gas density  $\langle n \rangle = 320 \text{ cm}^{-3}$ , according to the Larson relations (Larson 1981; Solomon et al. 1987) and to  $\mathcal{M} \approx 10$ . Although ionization by UV photons is generally important at this relatively low density (and likely low extinction), we

assume in the following that the gas is ionized by cosmic rays. We do so because, while the volume averaged gas density is relatively low, most of the gas is actually at densities larger than ten times the mean density, due to the very intermittent density distribution (Padoan et al. 1998; Padoan & Nordlund 1999). In numerical experiments with  $\mathcal{M} \approx 10$  and numerical mesh size of  $128^3$ , the complex system of interacting shocks generates a very large density contrast of almost six orders of magnitude ( $0.1 \text{ cm}^{-3} \lesssim n \lesssim 10^5 \text{ cm}^{-3}$ ). However, the ambipolar drift heating rate computed in this work and expressed in eqn. (25) can be rescaled to any value of the average gas density, and it is increasingly accurate for increasing average density, because of the assumption of cosmic ray ionization.

Cosmic rays ionization results in the following expression for the fractional ionization  $x_i$ :

$$x_i \equiv \frac{K_i}{n_n^{1/2}} \quad (13)$$

where  $n_n$  is the number density of neutrals, and  $K_i$  is of order  $10^{-5} \text{ cm}^{-3/2}$  (see the discussion of  $K_i$  in McKee et al. 1993). We have not included photoionization by the ambient radiation field, although it is important at low extinction (McKee 1989). Equation (13) underestimates the ionization, and hence overestimates the degree of ambipolar drift, in the low density gas, but our main interest is in the high density regions, which contain most of the mass.

In order to explain our parameterization of ambipolar drift, we must introduce our natural units and nondimensionalized equations. We denote quantities defining a unit by a subscript  $u$  and dimensionless quantities by tildes, that is  $\tilde{\mathbf{B}} = \mathbf{B}/B_u$ ,  $\tilde{\mathbf{v}} = \mathbf{v}/v_u$ ,  $\tilde{\mathbf{J}} = \tilde{\nabla} \times \tilde{\mathbf{B}}$ ,  $\tilde{\nabla} = L_u \nabla$ , and  $\tilde{n} = n/n_u$ . The code is written so that the units are:

$$B_u = c_S(4\pi\langle\rho\rangle)^{1/2} \quad (14)$$

$$v_u = c_S \tag{15}$$

$$n_u = \langle n \rangle \tag{16}$$

$$L_u = L/N \tag{17}$$

where  $c_S$  is the sound speed,  $L$  the physical size of the simulation box, and  $N$  the linear resolution of the numerical box.

The ambipolar drift velocity is written as

$$\tilde{\mathbf{v}}_D = a\tilde{n}^{-3/2}\tilde{\mathbf{J}} \times \tilde{\mathbf{B}} \tag{18}$$

The ambipolar drift parameter  $a$  can be computed from the expression  $\tilde{\mathbf{v}}_D = \mathbf{v}_D/v_u$ , and using equation (4) and (18), together with (14), (15),(16) and (17). The result is:

$$a = 0.28 \left(\frac{T}{10K}\right)^{1/2} \left(\frac{N}{128}\right) \left(\frac{L}{10 \text{ pc}}\right)^{-1} \left(\frac{\langle n \rangle}{200 \text{ cm}^{-3}}\right)^{-1/2} \left(\frac{K_i}{10^{-5} \text{ cm}^{-3/2}}\right)^{-1} \left(\frac{\langle \sigma v \rangle}{2 \times 10^{-9} \text{ cm}^3 \text{ s}^{-1}}\right)^{-1}. \tag{19}$$

The value of the parameter  $a$  that we use in most of the present experiments is  $a = 0.3$  in  $128^3$  runs, and appropriately rescaled for different resolutions. Using equation (19),  $a = 0.3$  corresponds to physical conditions in typical molecular clouds with temperature  $T = 10$  K, size  $L = 10$  pc, and volume averaged number density  $\langle n \rangle = 200 \text{ cm}^{-3}$ . Using Larson’s relation between size and density (Larson 1981; Solomon et al 1987),  $\langle n \rangle \propto L^{-1}$ , the dependence of  $a$  on the cloud size would be  $a \propto L^{-1/2}$ . As an example, a cloud or cloud core with  $L = 1$  pc and  $\langle n \rangle = 2000 \text{ cm}^{-3}$ , would require a value of  $a = 0.88$ , while a

giant molecular cloud complex with  $L = 50$  pc should be modeled with  $a = 0.12$ . Physical conditions in molecular clouds with sizes in the range 1–50 pc can therefore be reproduced numerically with values of  $a$  within a factor of less than 3 from the value  $a = 0.3$  (at  $N = 128^3$  resolution) adopted in most of the numerical experiments used in this work. However, the dependence of the ambipolar drift heating rate on the parameter  $a$  has been computed (see Figure 5), by varying the value of  $a$  in the simulations in the range  $0.15 \leq a \leq 1.0$ , that corresponds to cloud size  $0.5 \text{ pc} \lesssim L \lesssim 50 \text{ pc}$ .

#### 4. The Ambipolar Drift Heating Rate

Our results are based on a variety of both driven and decaying cloud models, over a range of parameters and at different resolutions, as described in the previous section. The heating rates that we report in the driven models all apply to the steady state, which is reached after approximately 3-4 dynamical times. However, because all quantities fluctuate slightly with time with respect to their steady state values, we typically enter values from several adjacent time slices of each simulation on the figures which follow.

Although, as we show later in this section, the heating rate varies considerably from point to point, the volume averaged heating rate  $\langle H_{AD} \rangle$  scales with the properties of the system in a remarkably simple way. We define the mean of a quantity  $Q$ ,  $\langle Q \rangle$ , by

$$\langle Q \rangle \equiv N^{-1} \sum_{ijk} Q_{ijk}, \quad (20)$$

where  $ijk$  indexes a grid point. From eqn. (6),

$$\langle H_{AD} \rangle = N^{-1} \sum_{ijk} (\rho_i \nu_{in} | \mathbf{v}_D |^2)_{ijk}, \quad (21)$$

where  $\mathbf{v}_D$  is computed from eqn. (4).

We have performed a convergence study of the dependence of  $\langle H_{AD} \rangle$  on numerical resolution. Figure 1 shows  $\langle H_{AD} \rangle$  for four simulations with  $N = 16^3, 32^3, 64^3,$  and  $128^3$ , and shows clear evidence for convergence, probably to better than a factor of 2, of the value found for the highest resolution.

Studies at high spatial resolution have shown that ambipolar drift can steepen the current density profile to the point that it virtually becomes singular (Brandenburg & Zweibel 1994, 1995, Mac Low et al 1995, Zweibel & Brandenburg 1997, Mac Low & Smith 1997). However, the contribution of such structures to the total heating rate is small, as shown by the following argument. The magnetic field varies with position  $x$  across a sheet as  $B \sim x^{1/3}$ , so  $J$  varies as  $x^{-2/3}$ . From eqns. (4) and (6),  $H_{AD} \propto x^{-2/3}$ , which is singular, but integrable: the integrated value of  $H_{AD}$  depends on the width  $x_s$  of the sheet as  $x_s^{1/3}$ . Therefore, these very thin structures contribute little to the heating rate - even less if one takes into account two fluid effects, which resolve the singularity.

Assuming that the heating rate is nearly converged, the scaling law we find for  $\langle H_{AD} \rangle$  depends on the mean magnetic field magnitude  $\langle |B| \rangle$

$$\langle |B| \rangle \equiv \langle (B^2)^{1/2} \rangle, \quad (22)$$

the rms velocity  $v_{rms}$

$$v_{rms} \equiv \langle v^2 \rangle^{1/2}, \quad (23)$$

and the Alfvén Mach number in the evolved state

$$\mathcal{M}_A \equiv \frac{v_{rms}(4\pi\langle\rho\rangle)^{1/2}}{\langle |B| \rangle}. \quad (24)$$

Figure 2 shows  $\langle H_{AD} \rangle / \mathcal{M}_A^2$  plotted versus  $\langle |B| \rangle$  for a set of simulations with constant sonic Mach number  $\mathcal{M} = 10$ . Thus,  $\mathcal{M}_A \propto \langle |B| \rangle^{-1}$  with a unique constant of proportionality, so we plot  $\mathcal{M}_A$  on the top axis of the figure. In all of these runs, the ambipolar drift parameter

$a$  defined in eqn. (19) is fixed at 0.3 for  $N = 128^3$ . According to the Larson relations, this model corresponds to a cloud with  $L \sim 6$  pc,  $\langle n \rangle \sim 320 \text{ cm}^{-3}$ .

Figure 2 shows a remarkably tight correlation between  $\langle |B| \rangle$  and  $\langle H_{AD} \rangle$ . The simulations are fit by the relation

$$\langle H_{AD} \rangle = 3.0 \times 10^{-24} \left( \frac{\langle |B| \rangle}{10 \mu G} \right)^4 \left( \frac{\mathcal{M}_A}{5} \right)^2 \left( \frac{\langle n \rangle}{320 \text{ cm}^{-3}} \right)^{-3/2} \text{ erg cm}^{-3} \text{ s}^{-1}, \quad (25)$$

which is shown as a solid line on Figure 2.

The cosmic ray heating rate  $H_{cr}$  corresponding to a primary cosmic ray ionization rate  $\zeta = 10^{-17} \text{ s}^{-1}$  is also plotted in Figure 2. Ambipolar drift heating exceeds cosmic ray heating unless the magnetic field is less than about  $3 \mu \text{ G}$ . However, the value  $\langle n \rangle = 320 \text{ cm}^{-3}$  has been used in Figure 2; for increasing values of the average gas density, the cosmic ray heating rate increases, since it is proportional to the gas density. The cosmic ray heating rate is also found to vary considerably from cloud to cloud, and could span the range of values  $10^{-16} \text{ s}^{-1} \lesssim \zeta \lesssim 10^{-18} \text{ s}^{-1}$  (Caselli et al. 1998; Williams et al. 1998).

Equation (6) is only compatible with eqn. (25) if

$$\langle L_B \rangle \equiv \left\langle \left( \frac{c^2 B^2}{(4\pi J)^2} \right)^{1/2} \right\rangle \propto \mathcal{M}_A^{-1}. \quad (26)$$

Figure 3 shows that this is in fact the case, unless  $\mathcal{M}_A > 10$ . For  $\mathcal{M}_A > 10$ , although the value of the volume averaged magnetic length scale,  $\langle L_B \rangle$ , is still a bit larger than the numerical grid scale, local values of  $L_B$  are so small that in many locations  $L_B$  is not resolved by the  $128^3$  numerical mesh. It is possible that  $\langle L_B \rangle \propto \mathcal{M}_A^{-1}$  also for  $\mathcal{M}_A > 10$ , but this cannot be shown in numerical runs with the present resolution.

Qualitatively, it is not surprising that  $\langle L_B \rangle$  decreases with increasing  $\mathcal{M}_A$ , or increasingly dominant kinetic energy. The larger  $\mathcal{M}_A$  is, the more the flow can bend the field, leading to more tangling and smaller  $L_B$ . What perhaps is surprising is that in cases

in which the field is initially weak, it is not amplified up to equipartition: if it were, there would be no points in Figure 3 with  $\mathcal{M}_A > 1$ . A number of factors can lead to saturation of the field below equipartition. The weaker the field is initially, the more it must be stretched and tangled to amplify it up to equipartition. The more tangled the field becomes, the more subject it is to numerical and ambipolar diffusion. It has also been shown (Brandenburg & Zweibel 1994, Brandenburg et al 1995, Zweibel & Brandenburg 1997) that ambipolar drift drives the magnetic field to a nearly force free state. Since the flow cannot do work on a force free field, amplification ceases once the force free state is reached. And finally, the magnetic field becomes quite spatially intermittent (see Figure 7), and locally strong Lorentz forces might feed back on the flow and quench the growth of the field even before ambipolar drift has had enough time to act.

The foregoing results on  $\langle H_{AD} \rangle$  and the behavior of  $\langle L_B \rangle$  are shown in another form in Figure 4, which is based on a decaying run with no driving and no mean magnetic field. The magnetic and kinetic energies are initially in equipartition, and remain so as they decrease with time. The magnetic field strength shown on the abscissa parameterizes time from late to early. Figure 4 shows that the sonic Mach number  $\mathcal{M}$  decays while  $\langle L_B \rangle$  and  $\mathcal{M}_A$  remain roughly constant. Despite fluctuations,  $\langle H_{AD} \rangle$  is proportional to  $\langle |B| \rangle^4$  as the magnetic field decays by an order of magnitude.

We have also studied the dependence of  $\langle H_{AD} \rangle$  on the ambipolar drift parameter  $a$ . Taken at face value, eqn. (6) predicts  $\langle H_{AD} \rangle \propto a$ . But this reasoning does not account for the dependence of the magnetic field properties on  $a$ . As  $a$  increases, the increase in magnetic diffusion decreases the efficiency with which the field is amplified, and increases  $L_B$ . The net result is that although  $\langle H_{AD} \rangle$  is positively correlated with  $a$ , the dependence is weaker than linear over the range of  $a$  which we have examined.  $H_{AD}$  and  $L_B$  are plotted versus  $a$  in Figure 5. The plot of  $\langle H_{AD} \rangle$  versus  $a$  is reasonably well fit by  $\langle H_{AD} \rangle \propto a^{0.6}$



over the limited but physically reasonable range  $0.15 \leq a \leq 1.0$ . The increase in  $\langle L_B \rangle$  by roughly a factor of 2 over this range of  $a$  accounts for the increase of  $\langle H_{AD} \rangle$  by roughly a factor of 4 instead of a factor of 7, as would occur for linear dependence.

Ambipolar drift makes a significant contribution to the rate at which the turbulence decays. Writing the kinetic energy  $E_K$  as

$$E_K = \frac{1}{2} \langle \rho \rangle v_{rms}^2 = \mathcal{M}_A^2 \frac{\langle |B| \rangle^2}{8\pi} \quad (27)$$

and using eqn. (25) we find the decay time  $\tau_{AD}$

$$\tau_{AD} \equiv \frac{E_K}{\langle H_{AD} \rangle} = 1.3 \times 10^6 \left( \frac{\langle |B| \rangle}{10 \mu\text{G}} \right)^{-2} \left( \frac{\langle n \rangle}{320 \text{ cm}^{-3}} \right)^{3/2} \text{ yr}. \quad (28)$$

For comparison, in these models the dynamical time scale  $L/v_{rms}$  is about  $2.4 \times 10^6$  yr. Thus, as has been argued elsewhere, ambipolar drift is an efficient mechanism for the dissipation of turbulent energy in molecular clouds (Zweibel & Josafatsson 1983, Elmegreen 1985).

Recently, it has been shown that supersonic hydrodynamic and hydromagnetic turbulence both decay as  $E_K \propto t^{-\eta}$ , with  $\eta \sim 1$  (Mac Low et al 1998, Mac Low 1999). This decay law implies

$$\frac{dE_K}{dt} \propto -E_K^2. \quad (29)$$

In these models, dissipation occurs primarily in shocks and through the generation and numerical dissipation of short wavelength Alfvén waves; there is no ambipolar drift.

Ambipolar drift actually leads to a similar decay law:  $\langle H_{AD} \rangle \propto \langle |B| \rangle^2 v_{rms}^2$ , which can be written as  $E_K^2$  since the ratio of magnetic to kinetic energy is fixed in these decaying models, as shown in Figure 4. Does it matter whether energy is lost by ion-neutral friction or in shocks? From an observational point of view it does matter, since the peak temperatures and spatial distribution of the heating in the two cases can be quite different.

We will explore this issue further in a study of thermal equilibrium in molecular clouds heated by ambipolar drift (Juvela et al. 2000).

Having established the mean properties, we now describe the pointwise properties of ambipolar drift heating. Figure 6 is a scatter plot, in dimensional units, of  $H_{AD}$  versus  $4\pi B^2 v^2 \rho^{-1/2}$  for points at which the density satisfies the condition  $n > 2\langle n \rangle$ . We choose to look only at relatively dense regions since we probably overestimate the ambipolar drift rate at low densities due to our choice of ionization law, eqn. (13). Moreover, we have plotted only a randomly selected subset of the points that satisfy the density condition, because there are so many points in the simulation that plotting all of them would produce a completely saturated, solid black clot. The solid line in Figure 6, which is the mean heating relation given in eqn. (25), is an approximate fit to the data, but there is a dispersion of a few orders of magnitude in the heating rates from point to point.

Figure 7 shows images of two-dimensional slices of  $H_{AD}$  (left panel) and  $\rho$  (right panel), both plotted on a grey scale corresponding to (magnitude)<sup>0.1</sup>. Figure 7 shows that both the heating and density distributions are highly inhomogeneous and filamentary, and that high density features are generally regions of strong heating. Bearing in mind that  $H_{AD} \propto \rho^{-3/2}$ , we see that the strong heating in high density regions must be a consequence of the  $B - \rho$  correlation and also the small values of  $L_B$  associated with thin, magnetized filaments.

A close examination of the heating and density distributions in Figure 7 shows thin local minima in the heating sandwiched between adjacent ribbons of strong heating. This phenomenon is seen more easily in Figure 8, which shows ambipolar drift heating and cosmic ray heating on a cut taken through the images shown in Figure 7. We have chosen to plot  $H_{CR}$ , which is linear in  $\rho$ , as a proxy for the density because this makes it easy to compare the relative magnitudes of ambipolar drift and cosmic ray heating. It is clear that density peaks are often flanked by peaks of  $H_{AD}$ . The reason for this is not hard

to understand. The magnetic field tends to be aligned with the density filaments, due to the strong compression which formed the filaments. Within the filaments, the drift velocity  $\mathbf{v}_D \propto -\nabla B^2 \propto \nabla \rho$ . According to eqn. (6), the heating reaches a minimum at the center of the filament and peaks off center where the density gradient is largest. Although the correlation between  $L_B$  and  $n$  shows considerable scatter, there is substantial correspondence between the most pronounced features in each, as shown in Figure 9.

The mean values of  $H_{CR}$  and  $H_{AD}$  are also plotted in Figure 8. In this model, with  $\langle |B| \rangle \approx 6\mu$  G, ambipolar drift heating is on average almost 4 times larger than cosmic ray heating.

## 5. Discussion and Conclusions

It was suggested some time ago that ambipolar drift, whether arising from the diffusion of a large scale magnetic field or from damping small scale turbulence, could be an important heating mechanism for molecular clouds (Scalo 1977, Goldsmith & Langer 1978, Zweibel & Josafatsson 1983). It was also pointed out in these papers that the observed low temperatures of molecular clouds implies bounds on the magnitude of the magnetic field, and/or the amplitude of the turbulence.

In practice, however, the magnitude of the ambipolar drift heating  $H_{AD}$  has been difficult to assess. Simple arguments show that  $H_{AD}$  should scale as  $B^4/(L_B^2 \rho \rho_i)$  (or  $B^4/(L_B^2 \rho^{3/2})$  for a cloud ionized by cosmic rays). The extreme sensitivity of  $H_{AD}$  to  $B$ , which at best can be measured only along the line of sight, and to the magnetic length scale  $L_B$ , which cannot be measured at all, make it difficult to estimate  $H_{AD}$  reliably to better than an order of magnitude. This has made ambipolar drift heating appear less attractive than mechanisms which can be reliably evaluated, such as heating by low energy cosmic

rays. It has also seriously weakened the constraints on magnetic field properties which arise from thermal balance calculations. The further difficulty of calculating radiative cooling rates which account self consistently for the turbulent structure of the cloud, including the effects of turbulence on cloud chemistry, has only compounded the problem.

For several reasons, the role of ambipolar drift heating in the thermal equilibrium of clouds is becoming more open to assessment, and hence more interesting. Reliable maps of temperature, density, magnetic field, and velocity structure are now available for more clouds than ever before, permitting correlation studies of cloud temperature with other properties. Detailed numerical models of turbulent molecular clouds, and improved calculations of cooling rates and cloud chemistry, are now feasible. Thermal balance calculations which include ambipolar drift heating, compared with observations, can now lead to meaningful diagnostics of magnetic fields and dynamical properties of molecular clouds.

In this paper we have used simulations of turbulent, magnetized molecular clouds to study the properties of heating by ambipolar drift. The models are self consistent in the sense that we include ambipolar drift in calculating the dynamics of the cloud and the evolution of the magnetic field. We have found that a realistic amount of ambipolar drift in a simulation with the highest numerical resolution practical for us ( $N = 128^3$  mesh points) imparts a physical as opposed to numerical diffusivity to the cloud which makes it just possible to capture all of the relevant length scales. The models can be scaled to approximate the sizes, densities, velocity dispersions, and magnetic field strengths of observed clouds. As our simulations do not include self gravity, we focus on ambipolar drift heating due to turbulence rather than due to the systematic redistribution of a large scale field in quiescent, gravitationally contracting structures.

The main result of our paper is an empirical formula for the volume averaged heating

rate,  $\langle H_{AD} \rangle$ , given in eqn. (25) :  $\langle H_{AD} \rangle \propto \langle |B| \rangle^4 \mathcal{M}_A^2 / \rho \rho_i$ , or  $\langle H_{AD} \rangle \propto \langle |B| \rangle^2 v_{rms}^2 / \rho_i$ . As shown in Figure 2, the fit is very good, and comes about because the magnetic length scale  $L_B$  is inversely proportional to  $\mathcal{M}_A$  (Figure 3). Our scaling law for  $\langle H_{AD} \rangle$  makes it possible to estimate the ambipolar drift heating rate in individual clouds much more accurately than before: the uncertainty in the value of  $B$  is only squared, not raised to the fourth power, and  $L_B$  is replaced by the more readily measurable rms velocity, or line width.

Furthermore,  $\langle H_{AD} \rangle$  turns out to be interestingly large, exceeding, for moderately large field strength, the mean cosmic ray heating rates  $H_{CR}$ . And, the turbulent dissipation times associated with ambipolar drift heating are of order the dynamical crossing times in our models, suggesting, as argued elsewhere, that the turbulence in molecular clouds must be driven continuously.

In some respects, however, the conventional wisdom that  $H_{AD}$  is difficult to estimate is borne out by its large range in value from point to point within any particular model. Despite the excellent correlation of the global heating rate with averaged quantities, a scatter plot of  $H_{AD}$  versus the pointwise values of the same quantities which go into the mean relation eqn. (25) shows dispersion of a few orders of magnitude about the mean, as shown in Figure 6, (although the relation based on global averages is an approximate fit to the centroid of the distribution). In models with a fairly weak magnetic field and a tight  $B - \rho$  relation, the correspondence between density and  $H_{AD}$  is quite good, even down to individual features (Figure 7).

We are presently studying the thermal equilibrium problem with a Monte Carlo treatment of radiative transfer. For the present, however, we note that standard calculations of radiative cooling rates in the temperature and density regimes of interest to us here ( $T \sim 10K - 40K$ ,  $n \sim 10^3 - 10^4$ ) scale with temperature as  $T^{2.2-2.7}$  (Goldsmith & Langer 1978, Neufeld, Lepp, & Melnick 1995). Therefore, if ambipolar drift is the dominant

heating mechanism, there should be a relation with temperature and line width of the form  $T \propto \Delta v^{.74-.91}$ . The exponent of this relation could be reduced, due to the dependence of the cooling rate on the velocity gradient in the gas. In fact, a positive correlation, but with a somewhat shallower slope, has recently been reported (Jijina, Myers, & Adams 1999). In general, however, we would expect that any model in which the dissipation of turbulence contributes to heating would produce a positive  $T - \Delta v$  correlation.

We thank Ted Bergin, Alyssa Goodman, Mika Juvela and Phil Myers for reading the manuscript and providing useful comments. We are happy to acknowledge support by NSF Grant AST 9800616 and NASA Grant NAG5-4063 to the University of Colorado, and support by the Danish National Research Foundation through its establishment of the Theoretical Astrophysics Center.

## REFERENCES

- Brandenburg, A., Nordlund, A., Stein, R.F., & Torkelsson, U. 1995, *ApJ*, 446, 741
- Brandenburg, A. & Zweibel, E.G. 1994, *ApJ*, 427, L91
- Brandenburg, A. & Zweibel, E.G. 1995, *ApJ*, 448, 734
- Caselli, P., Walmsley, C.M., Terzieva, R., Herbst, E. 1998, *ApJ*, 499, 234
- de Jong, T., Dalgarno, A., & Boland, W. 1980, *A&A*, 91, 68
- Draine, B.T. 1980, *ApJ*, 241, 1021
- Draine, B.T. 1986, *MNRAS*, 220, 133
- Draine, B.T. & McKee, C.F. 1993, *ARA&A*
- Draine, B.T., Roberge, W. G., & Dalgarno, A. 1983, *ApJ*, 264, 485
- Elmegreen, B.G. 1985, *ApJ*, 299, 196
- Galsgaard, K., Nordlund, Å. 1996, *Journal of Geophysical Research*, 101(A6), 13445
- Galsgaard, K., Nordlund, Å. 1997, *Journal of Geophysical Research*, 102, 231
- Goldreich, P. & Kwan, J. 1974, *ApJ*, 189, 441
- Goldsmith, P.F. & Langer, W.D. 1978, *ApJ*, 222, 881
- Hawley, J.F. & Stone, J.M. 1998, *ApJ*, 501, 758
- Hyman, J. 1979, in R. Vichnevetsky, R. S. Stepleman (eds.), *Adv. in Comp. Meth. for PDE's—III*, 313
- Jijina, J., Myers, P. C., & Adams, F. C. 1999, *ApJS*, in press
- Juvela, M., Padoan, P., Nordlund, A., & Zweibel, E.G. 2000 to be submitted to *ApJ*
- Kolmogorov, A. N. 1941, *Dokl. Akad. Nauk. SSSR*, 30, 301

- Larson, R.B. 1981, MNRAS, 194, 809
- Mac Low, M.-M., Norman, M.L., Kónigl, A., & Wardle, M. 1995, ApJ, 442, 726
- Mac Low, M.-M., & Smith, M.D. 1997, ApJ, 491, 596
- Mac Low, M.-M., Klessen, R.S., Burkert, A., Smith, M.D., & Kessel, O. 1998, in J. Franco, A. Carramiñana (eds.), *Interstellar Turbulence*, Cambridge University Press
- Mac Low, M.-M. 1999, ApJ, in press
- McKee, C.F. 1989, ApJ, 345, 782
- McKee, C.F., Zweibel, E.G., Heiles, C. & Goodman, A.A. 1993, in *Protostars & Planets III*, ed. E.H. Levy & J.I. Lunine, U. of Arizona Press, Tucson, 327
- Mullan, D.J. 1971, MNRAS, 153, 145
- Nakano, T. & Umebayashi, T. 1986, MNRAS, 218, 663
- Neufeld, D.A., Lepp, S., & Melnick, G.J. 1995, ApJ, 100, 132
- Nordlund, Å. & Galsgaard, K. 1997, A 3D MHD Code for Parallel Computers, Technical report, Astronomical Observatory, Copenhagen University
- Nordlund, Å., Stein, R.F., & Galsgaard, K. 1996, in J. Wazniewski (ed.), *Proceedings from the PARA95 workshop*, Vol. 1041 of *Lecture Notes in Computer Science*, Springer, p. 450
- Padoan, P., Juvela, M., Bally, J., & Nordlund, Å. 1998, ApJ, 504, 300
- Padoan, P. & Nordlund, Å. 1999, ApJ, in press
- Scalo, J.M. 1977, ApJ, 213, 705
- Scalo, J.M. & Pumphrey, W.A. 1982, ApJ, 258, L29
- Shu, F.H. 1983, ApJ, 273, 202
- Solomon, P.M., Rivolo, A.R., Barrett, J., & Yahil, A. 1987, ApJ, 319, 730



Stone, J.M., Ostriker, E.C., & Gammie, C.F. 1998, ApJ, 508, L99

Toth, G. 1994, ApJ, 425, 171

Williams, J.P., Bergin, A.B., Caselli, P., Myers, P.C., & Plume, R. 1998, ApJ, 503, 689

Zweibel, E.G. & Brandenburg, A. 1997, ApJ, 478, 563

Zweibel, E.G. & Josafatsson, K. 1983, ApJ, 270, 511

## FIGURE AND TABLE CAPTIONS

**Table 1:** Volume and time averaged parameters of the numerical experiments. In the case of the decaying experiment B1, the initial values of  $\langle |B| \rangle$  and  $\mathcal{M}$  are given, instead of their time averaged values.

**Figure 1:** Left panel: Volume averaged ambipolar heating rate per unit volume as a function of the average magnetic field strength, in snapshots from simulations with different size of the numerical mesh. The heating rate has been divided by its expected value (see §4) in a model with  $\mathcal{M}_A = 5$  and  $\langle |B| \rangle = 10 \mu\text{G}$ . Right panel: Heating rate averaged over the different snapshots used in the left panel, versus the linear size of the computational mesh. The heating rate shows a clear trend to convergence.

**Figure 2:** Volume averaged ambipolar drift heating rate, divided by the square of the rms Alfvénic Mach number, versus the averaged magnetic field strength, in randomly driven  $128^3$  simulations, with roughly constant ordinary rms Mach number,  $M \approx 10$ , and  $\langle n \rangle = 320 \text{ cm}^{-3}$ . The continuous line shows a  $\langle |B| \rangle^4$  dependence, while the dashed line is the cosmic ray heating rate per unit volume, also divided by  $\mathcal{M}_A^2$ .

**Figure 3:** Magnetic length scale (see text) versus the rms Alfvénic Mach number of the flow, in  $128^3$  simulations. The upper dashed line marks the physical size of the simulation box, and the lower dashed line the physical size that corresponds to the numerical resolution (taken as two grid cells). The continuous line shows a  $\mathcal{M}_A^{-1}$  dependence.  $L_B$  is roughly proportional to  $\mathcal{M}_A^{-1}$ , in a range of values of  $\mathcal{M}_A$  typical of conditions in molecular clouds, while it departs from that dependence around  $\mathcal{M}_A \approx 10$ , where  $L_B$  approaches the limit of the numerical resolution.

**Figure 4:** Volume averaged ambipolar drift heating rate per unit volume, divided by the square of the rms Alfvénic Mach number, versus the averaged magnetic field strength, in a decaying  $128^3$  simulation. The continuous line shows a  $\langle |B| \rangle^4$  dependence. Kinetic and magnetic energy decay at approximately the same rate, and so the flow is in approximate equipartition at all times,  $\mathcal{M}_A \approx 1$ . Also the magnetic length scale  $L_B$  is approximately constant, which proves that it depends only on  $\mathcal{M}_A$ .

**Figure 5:** Upper panels: Volume averaged ambipolar drift heating rate per unit volume, divided by its expected value for  $a = 0.3$ , according to eqn. (25). Different symbols represent different values of the ambipolar diffusion parameter,  $a$ . Lower panels: Magnetic lengthscale for different values of the ambipolar diffusion parameter.

**Figure 6:** Local value of the ambipolar drift heating rate per unit volume, versus its expected average value for the average parameters used in the simulation:  $\mathcal{M}_A = 5$ ,  $\langle |B| \rangle = 10 \mu\text{G}$ , and  $\langle n \rangle = 320 \text{ cm}^{-3}$ . The local heating rate spans a range of values of about 8 orders of magnitude, but it also follows the value expected for the volume averaged heating rate, shown by the continuous line. Only points with  $n > 2\langle n \rangle$  have been used in the scatter plot (see text).

**Figure 7:** Images of two-dimensional slices of ambipolar diffusion heating rate per unit volume (left) and of gas density (right), from a snapshot of a  $128^3$  simulation, with  $\mathcal{M}_A \approx 5$ , and  $\langle |B| \rangle \approx 6 \mu \text{ G}$ . The intensity in the image is proportional to  $H_{AD}^{0.1}$  (left) and  $n^{0.1}$  (right).

**Figure 8:** Local ambipolar drift heating rate (thick line) and cosmic ray heating rate

(thin line) per unit volume. It is a cut through the slice presented in Fig. 7. The dashed lines show the values of the heating rates averaged over the whole computational box.

**Figure 9:** Images of two-dimensional slices of magnetic length scale (left) and gas density (right). The slice is the same used in Fig. 7, and the intensity in the image is proportional to  $L_B^{0.1}$  (left) and  $n^{0.1}$  (right).

Model name	$\mathcal{M}_A$	$\langle  B  \rangle / \mu\text{G}$	$\mathcal{M}$	$a$	Size	Remarks
A1 .....	83.1	0.4	9.9	0.3	$128^3$	Driven
A2 .....	18.2	2.1	12.0	0.3	$128^3$	Driven
A3 .....	8.2	3.5	9.1	0.3	$128^3$	Driven
A4 .....	5.5	6.1	10.5	0.3	$128^3$	Driven
A5 .....	4.2	8.1	10.8	0.3	$128^3$	Driven
A6 .....	2.5	10.1	8.1	0.3	$128^3$	Driven
A7 .....	0.7	59.5	12.4	0.3	$128^3$	Driven
A4 <sub>16</sub> .....	5.3	5.1	8.5	0.0375	$16^3$	Driven
A4 <sub>32</sub> .....	4.0	6.3	8.0	0.075	$32^3$	Driven
A4 <sub>64</sub> .....	5.0	5.9	9.5	0.15	$64^3$	Driven
B1 .....	1.0	27.6	9.2	0.3	$128^3$	Decaying
A3 <sub>15</sub> .....	8.8	3.1	8.8	0.15	$128^3$	Driven
A3 <sub>6</sub> .....	10.6	3.1	10.5	0.6	$128^3$	Driven
A3 <sub>1.0</sub> .....	9.6	3.1	9.5	1.0	$128^3$	Driven

Table 1:

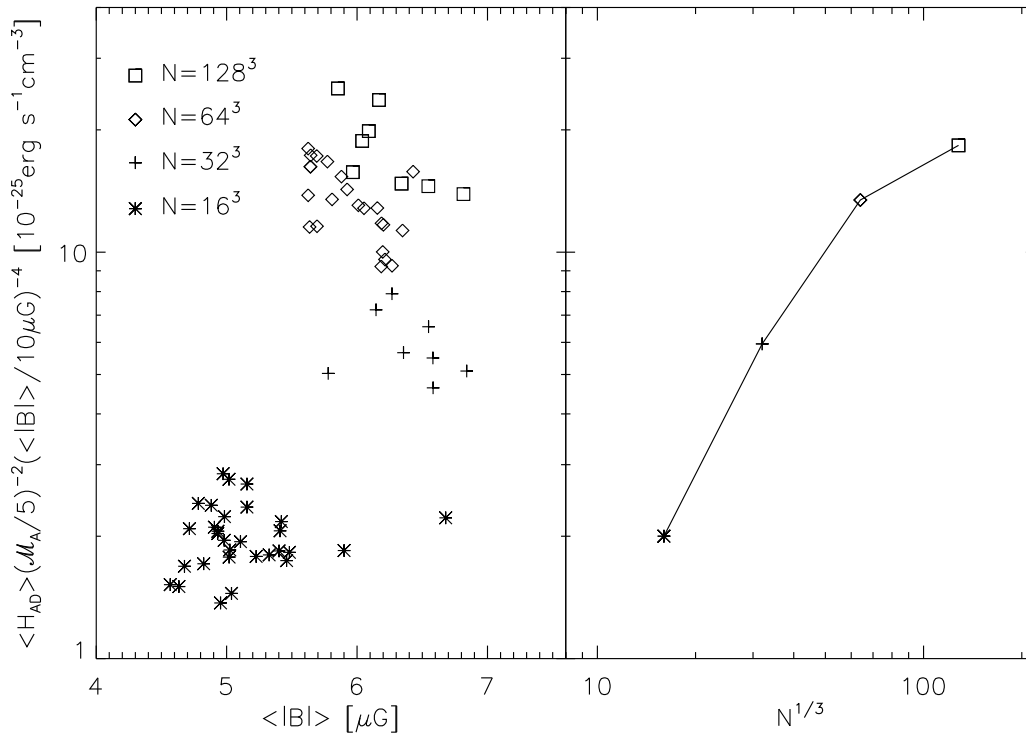


Fig. 1.—

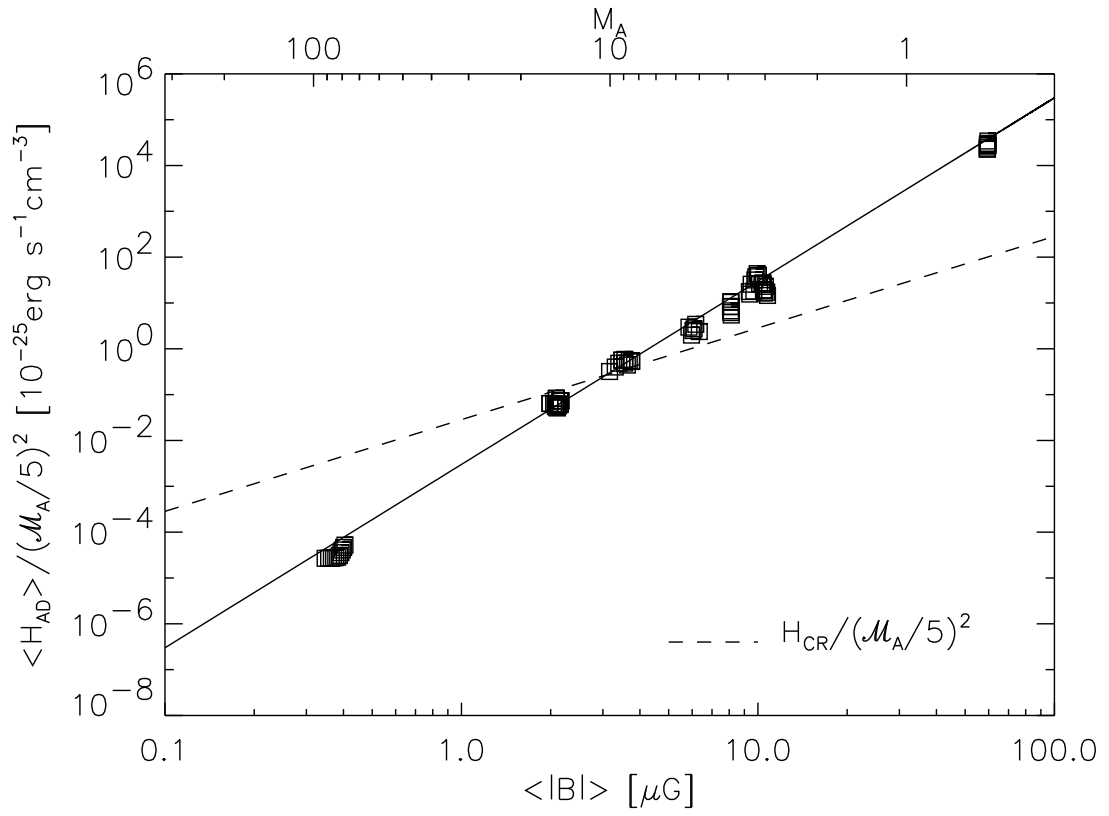


Fig. 2.—

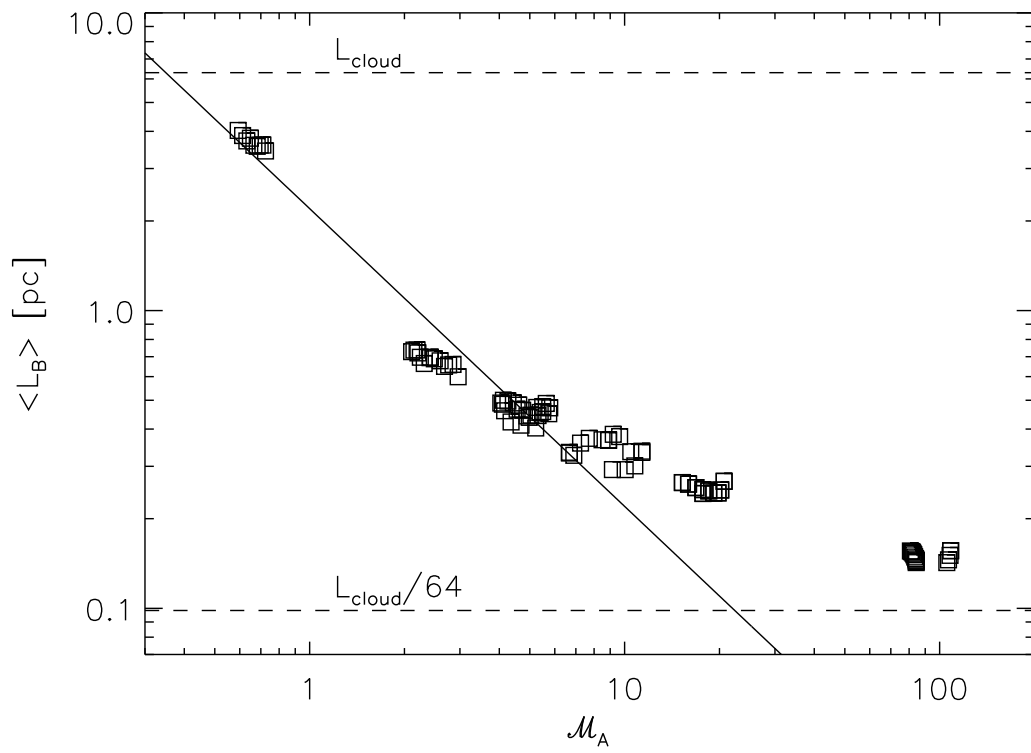


Fig. 3.—



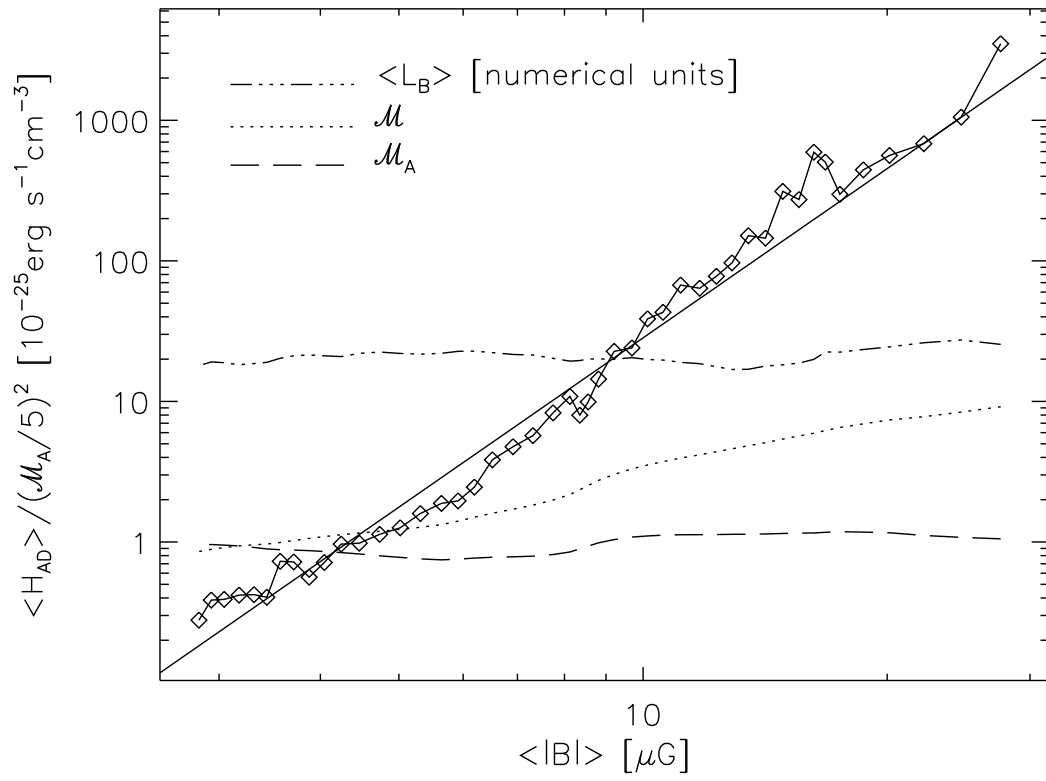


Fig. 4.—

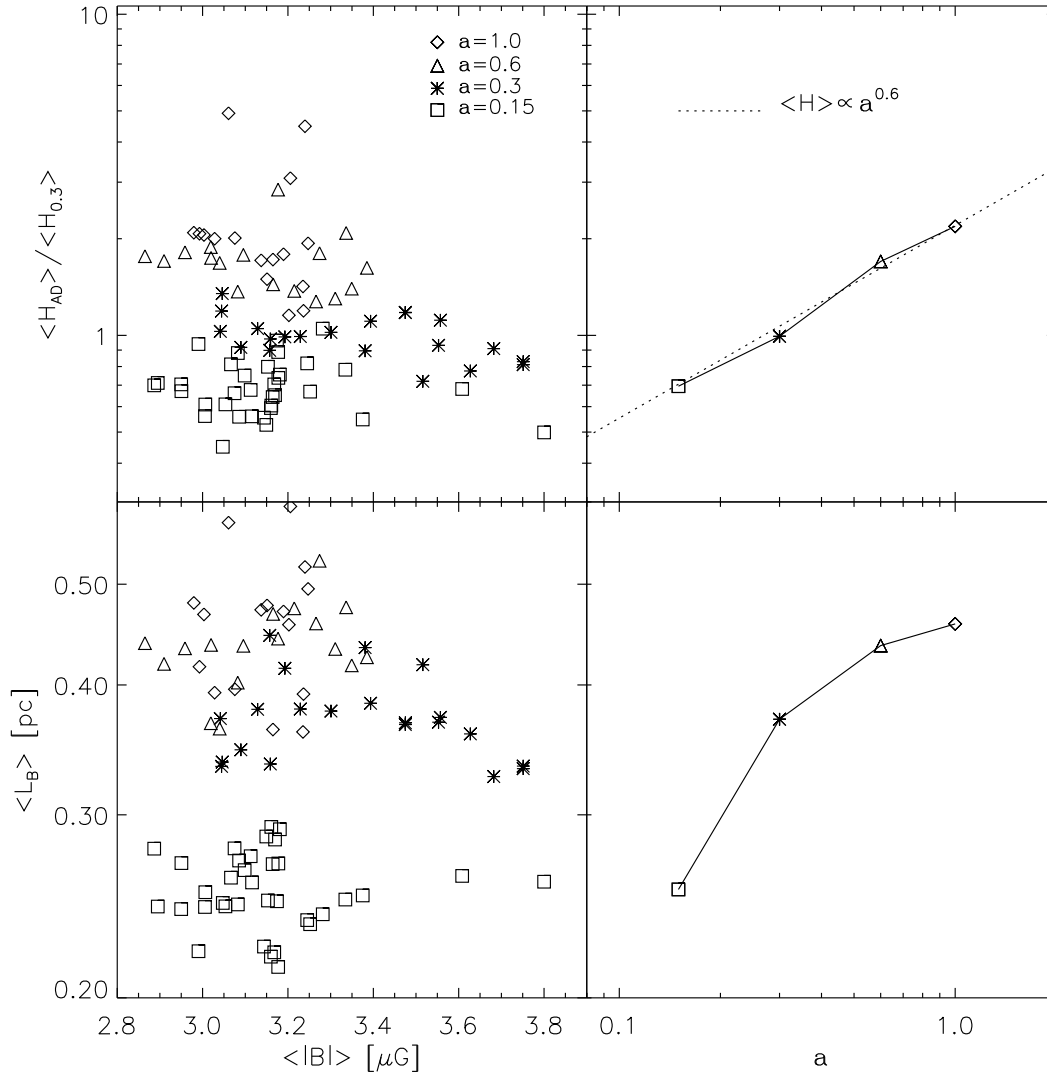


Fig. 5.—

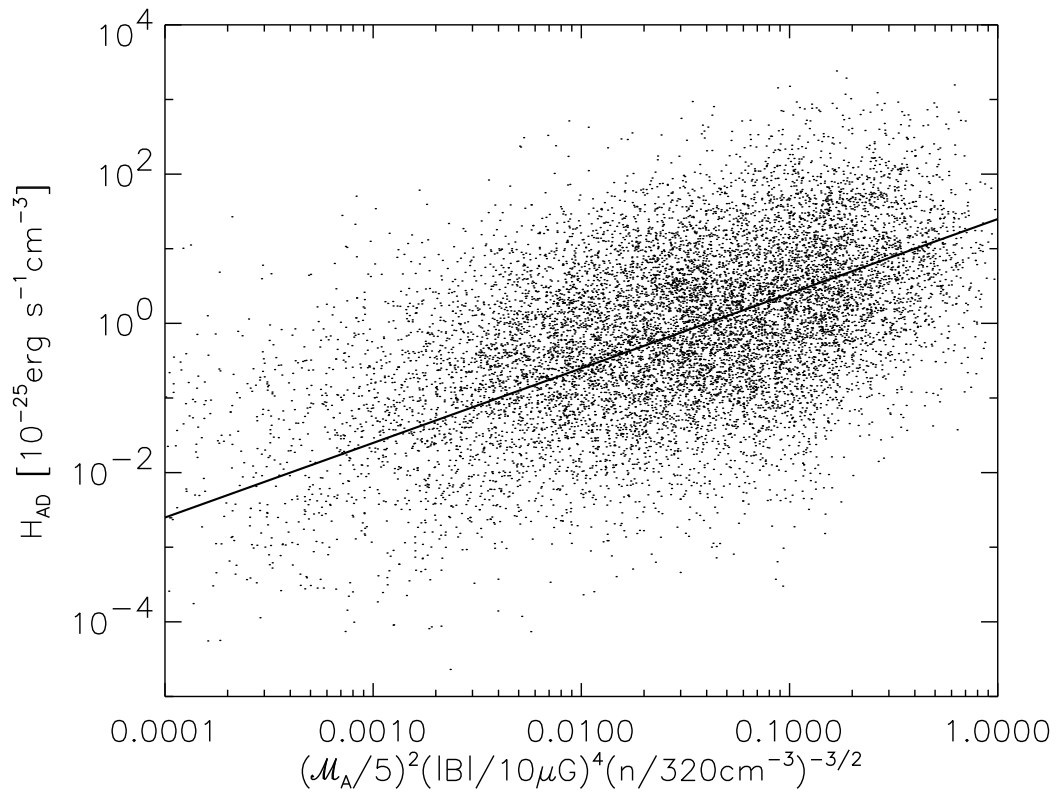


Fig. 6.—



Fig. 7.—

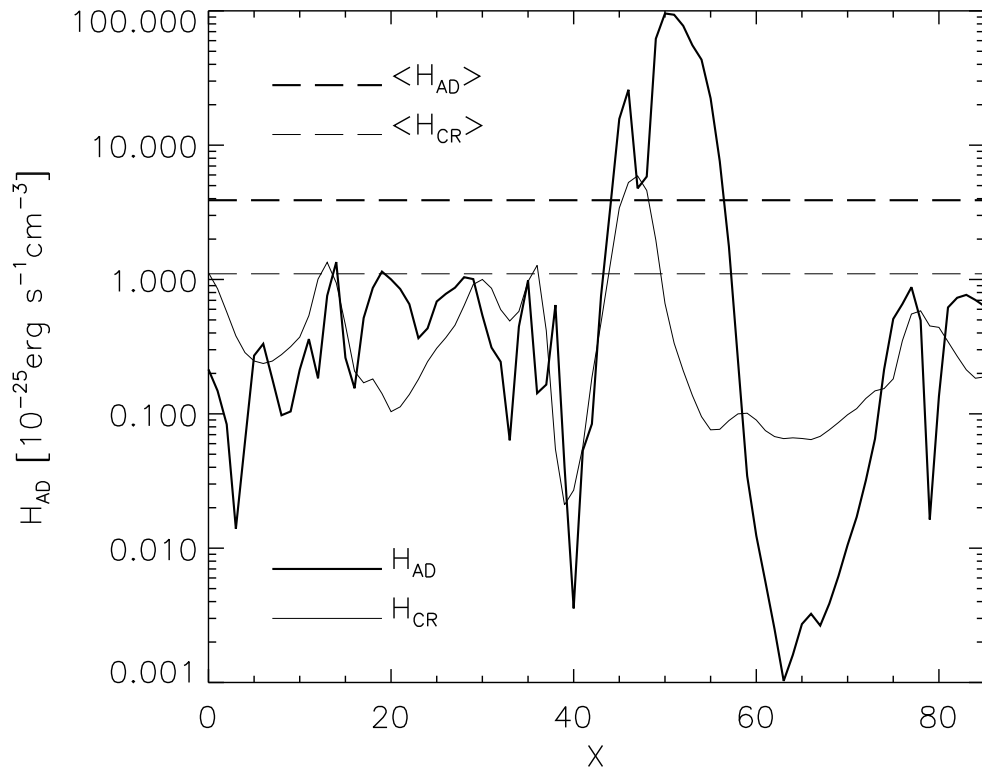


Fig. 8.—

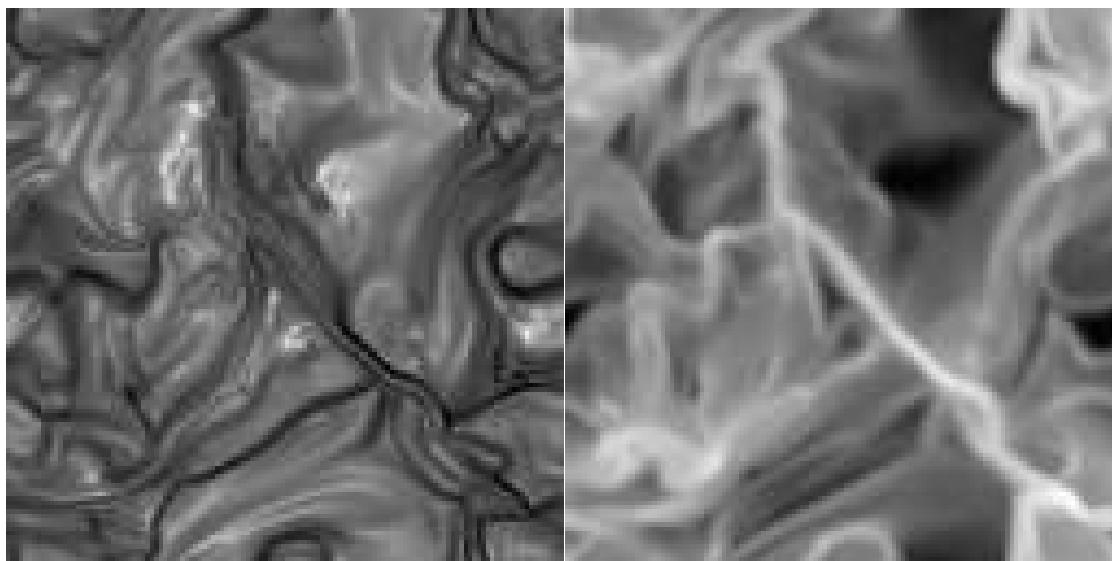


Fig. 9.—